Competing Roles of Ca2+and Nonmuscle Myosin IIA on the Dynamics of the Metastasis-Associated Protein S100A4

Yildirim, Ahmet; Tekpinar, Mustafa; Wassenaar, Tsjerk A.

Published in:
Journal of Physical Chemistry B

DOI:
10.1021/acs.jpcb.1c02096

Publication date:
2021

THE JOURNAL OF PHYSICAL CHEMISTRY B
A JOURNAL OF THE AMERICAN CHEMICAL SOCIETY

pubs.acs.org/JPCB

Article

Competing Roles of Ca^{2+} and Nonmuscle Myosin IIA on the Dynamics of the Metastasis-Associated Protein S100A4

Ahmet Yildirim,* Mustafa Tekpinar, and Tsjerk A. Wassenaar

Cite This: *J. Phys. Chem. B* 2021, 125, 10059–10071

Read Online

ACCESS | Metrics & More | Article Recommendations | Supporting Information

ABSTRACT: The calcium-binding protein S100A4 plays an important role in a wide range of biological processes such as cell motility, invasion, angiogenesis, survival, differentiation, contractility, and tumor metastasis and interacts with a range of partners. To understand the functional roles and interplay of S100A4 binding partners such as Ca^{2+} and nonmuscle myosin IIA (NMIIA), we used molecular dynamics simulations to investigate apo S100A4 and four holo S100A4 structures: S100A4 bound to Ca^{2+}, S100A4 bound to NMIIA, S100A4 bound to Ca^{2+} and NMIIA, and a mutated S100A4 bound to Ca^{2+} and NMIIA. Our results show that two competing factors, namely, Ca^{2+}-induced activation and NMIIA-induced inhibition, modulate the dynamics of S100A4 in a competitive manner. Moreover, Ca^{2+} binding results in enhanced dynamics, regulating the interactions of S100A4 with NMIIA, while NMIIA induces asymmetric dynamics between the chains of S100A4. The results also show that in the absence of Ca^{2+} the S100A4−NMIIA interaction is weak compared to that of between S100A4 bound to Ca^{2+} and NMIIA, which may offer a quick response to dropping calcium levels. In addition, certain mutations are shown to play a marked role on the dynamics of S100A4. The results described here contribute to understanding the interactions of S100A4 with NMIIA and the functional roles of Ca^{2+}, NMIIA, and certain mutations on the dynamics of S100A4. The results of this study could be interesting for the development of inhibitors that exploit the shift of balance between the competing roles of Ca^{2+} and NMIIA.

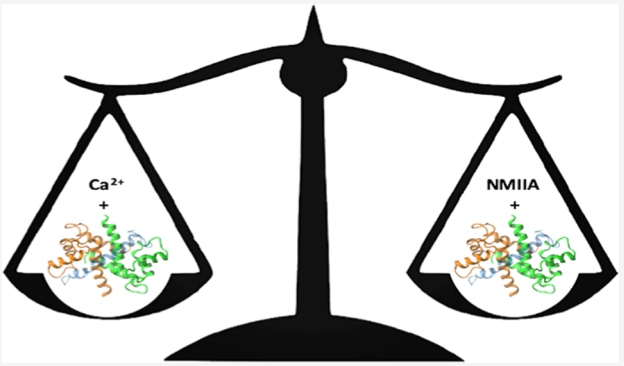

INTRODUCTION

Calcium ions are extensively used as second messengers in cellular processes, including cell migration, exocytosis, gene transcription, muscle contraction, and neurotransmitter release.[1,2] Intracellularly, signaling information is encoded in both amplitudes and frequencies of calcium oscillations. To translate these signals to cellular processes, the oscillations need to be decoded again. This is done by calcium-binding proteins that undergo calcium-induced conformational changes.[3,4] One such protein is S100A4, which is one of the 25 members of the S100 family of Ca^{2+}-binding proteins.

S100A4 is naturally expressed in both normal and cancer cells, and its increased level is correlated with cell motility. It is known that S100A4 is activated wherever cell migration is required for various biological processes including wound healing,[5] angiogenesis,[6] and cancer metastasis.[7] Thus, S100A4 is used as a marker for clinical prognosis in a number of cancers.[8−10] The overexpression of S100A4 leads to increased motility and migration of cells,[11,12] thus the metastatic spread of tumor cells in vivo,[13,14] whereas inhibition of S100A4 expression reduces the metastatic potential of tumor cells.[10,15] The correlation between the overexpression of S100A4 and metastasis was first detected in human breast cancer.[16] Numerous studies confirmed that the overexpression of S100A4 is also related to the metastasis of several types of cancers such as gastric,[17] prostate,[18,19] colon,[20] liver,[21] lung,[22] pancreatic,[23] gallbladder,[24] ovarian,[25] urinary bladder,[26] esophageal,[27] and thyroid carcinomas[28] as well as breast.[16]

Altogether, many studies show that the S100A4 protein plays a substantial role in metastatic spread of tumor cells. Unfortunately, little is still known about the molecular mechanisms underlying these processes. S100A4 has a homodimeric structure[29,30] and each monomer is composed of four helices, three loops, and two Ca^{2+} binding sites with a pseudo (N-terminal) and a canonical (C-terminal) EF-hand (Figure 1). In the absence of Ca^{2+}, helices 3 and 4 in each monomer exhibit a parallel orientation with respect to each other. However, Ca^{2+} binding to S100A4 reveals a hydrophobic binding pocket formed by helices 3, 4, the hinge region (residues 43−46) of loop 2, and the C-terminal coil region with significant conformational changes in the canonical EF-hand, with a ∼60° reorientation of helix 3 with respect to helix

Received: March 8, 2021
Revised: August 23, 2021
Published: August 31, 2021

https://doi.org/10.1021/acs.jpcb.1c02096
J. Phys. Chem. B 2021, 125, 10059−10071

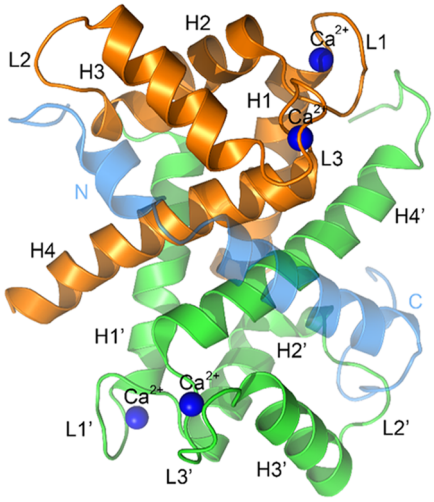

Figure 1. S100A4 crystal structure in complex with NMIIA peptide. Chains A and B are colored as orange and green, respectively, while Ca^{2+} is blue, and NMIIA is shown as transparent blue cartoons. All helices (H) and loops (L) are labeled in the figure. The figure was produced with PyMOL.[50]

4. This hydrophobic pocket serves as a binding site for the target proteins. As a result, the Ca^{2+}-free S100A4 is in a closed conformation (inactive state), but the Ca^{2+}-bound S100A4 is in an open conformation (active state) with a hydrophobic pocket formed by loop 2 and helix 3 and helix 4.[31−35] S100A4 interacts with nonmuscle myosin IIA (NMIIA), actin, rhotekin, and tropomyosin that are essential regulators of cell migration and invasion.[36] Interaction of S100A4 and NMIIA causes the filament disassembly of NMIIA, inhibits the filament assembly of monomeric NMIIA,[31,37−40] and enhances cell migration of metastatic tumor cells.[41] S100A4 complexes with 39 residues (Q1897−A1935) and 70 residues (A1868−G1938) fragments of NMIIA demonstrate structural similarities and S100A4 binds to NMIIA in an asymmetrical manner.[42] Pálfy et al. indicated that NMIIA binding increases the rigidity of helix 1 and Ca^{2+} affinity in S100A4 via allosteric conformational changes.[43] Another study showed that chemical shifts occur within the region immediately C-terminal to helix 4 upon addition of Ca^{2+} and N-terminal EF-hand has a higher binding affinity than C-terminal EF-hand.[44] Duelli et al. found that interactions between the positively charged residues of C-terminal and the negatively charged residues of Ca^{2+}-free S100A4 EF-hands have decreased upon Ca^{2+} binding.[45] Furthermore, an experimental study found that mutation of the C-terminal EF-hand of S100A4 reduces Ca^{2+} binding and cell motility/invasion in vitro and the affinity of the interaction of S100A4 and NMIIA isoform, and metastasis promotion.[46] Another study showed that the C-terminal lysine (residue 101) in wild-type S100A4 increases the rate of association between S100A4 and NMIIA isoform, suggesting that the C-terminal region of S100A4 is an important inhibitor-binding site for its metastasis-inducing properties.[46,47] Moreover, cysteine residues at the dimer surface of S100A4 in the extracellular space may form disulfide bonds when they are oxidized.[48,49]

Despite the wealth of structural information, our knowledge on the dynamics is quite limited. Insights into the molecular dynamics (MD) of S100A4 and the mechanisms controlling the (dis)assembly of NMIIA may contribute to the design of new inhibitors to disrupt the interaction of S100A4 with NMIIA to prevent the spread of tumor cells. To better understand the molecular mechanisms involved in S100A4−NMIIA interactions and the effect of calcium and disulfide bridges, we performed microsecond-long atomistic classical molecular dynamics simulations of five systems: wild-type S100A4 (WT S100A4), S100A4 bound to Ca^{2+} (S100A4 + Ca^{2+}), S100A4 bound to NMIIA (S100A4 + NMIIA), S100A4 bound to Ca^{2+} and NMIIA (S100A4 + Ca^{2+} + NMIIA), and mutated S100A4 (C3S/C81S/C86S/F45W) bound to Ca^{2+} and NMIIA (mutated S100A4 + Ca^{2+} + NMIIA).

MATERIALS AND METHODS

Starting Structures. The experimental structures of S100A4 were obtained from the protein data bank:[51] WT S100A4 (PDB ID: 1m31[34]), S100A4 bound to Ca^{2+} (PDB ID: 2q91[33]), S100A4 bound to NMIIA (3zwh[52]), S100A4 bound to Ca^{2+} and NMIIA (PDB ID: 3zwh[52]), and a four mutant S100A4 (C3S/C81S/C86S/F45W) bound to Ca^{2+} and NMIIA (PDB ID: 3zwh[52]). The mutagenesis wizard tool in PyMOL[50] was used to replace residues 3, 81, 86, and 45 in the mutated S100A4 with native amino acids. It should be noted that NMIIA used in all systems has 43 residues (Y1893-A1935).

MD Simulations. All simulations were carried out using GROMACS-2018.1 software.[53−57] In all simulations, we used the AMBER99SB-ILDN force field[58] for proteins, TIP3P model[59] for water molecules, the linear constraint solver (LINCS) algorithm[60] to constrain hydrogen bonds, and the SETTLE algorithm[61] to constrain bond lengths and angles of water molecules. We used the rhombic dodecahedron as a simulation box with periodic boundary conditions and a minimum distance of 1.2 nm between the solvent and the box for all systems. S100A4 in the systems contains residues 2−94. Na^+ and Cl^- ions were added to neutralize the systems and to obtain a physiological salt concentration of 150 mM. The leap-frog integrator method[62] was used to integrate the equations of motion with a time step of 2 fs. The temperature was held constant with V-rescale thermostat,[63] with a coupling constant of 1.0 ps and a reference temperature of 300 K. The pressure was coupled weakly and isotropically to a reference pressure using the Berendsen barostat[64] at 1 bar during the equilibrium step of the simulations, while the Parrinello−Rahman barostat[65] was used with a time constant of 1.0 ps and a compressibility of 4.5 × 10^{-5}/bar during the 1 μs long production simulations. Electrostatic interactions were modeled with the particle mesh Ewald (PME) algorithm,[66] a long-range cutoff value of 1.2 nm, and a grid spacing of 0.12 nm. As for the van der Waals interactions, a cutoff of 1.1 nm was used. After an initial minimization, a short equilibration procedure (1 ns) was conducted under constant volume and temperature. Afterward, a constant pressure and temperature equilibration was carried out for 1 ns. The production runs were also under constant pressure and temperature. Each production run was 1 μs long. All systems were simulated in three replicas; therefore, cumulative simulation time is 15 μs. More details about simulations are given in Table S1.

RESULTS AND DISCUSSION

Structural Stability of Proteins. To evaluate the structural stability of S100A4 structures, the root-mean-square deviation (RMSD) and root-mean-square fluctuation (RMSF) of C_α atoms were determined and analyzed. The overall

https://doi.org/10.1021/acs.jpcb.1c02096
J. Phys. Chem. B 2021, 125, 10059−10071

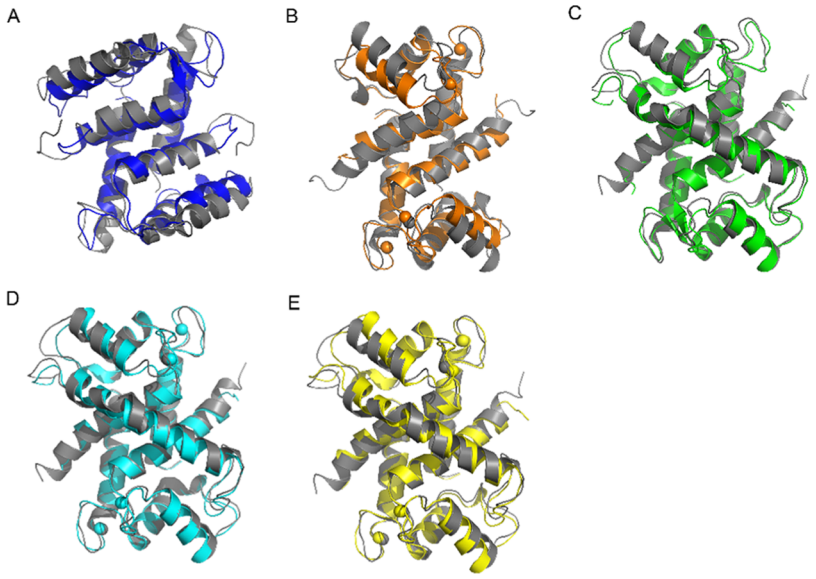

Figure 2. Superposition of C_α atoms of starting structures and MD-derived structures. (A) WT S100A4. (B) S100A4 bound to Ca^{2+}. (C) S100A4 bound to NMIIA. (D) S100A4 bound to Ca^{2+} and NMIIA. (E) Mutated S100A4 bound to Ca^{2+} and NMIIA. The starting structures are colored as gray. WT S100A4, S100A4 bound to Ca^{2+}, S100A4 bound to NMIIA, S100A4 bound to Ca^{2+} and NMIIA, and mutated S100A4 bound to Ca^{2+} and NMIIA are colored as blue, orange, green, cyan, and yellow, respectively. The names of the segments are shown in Figure 1.

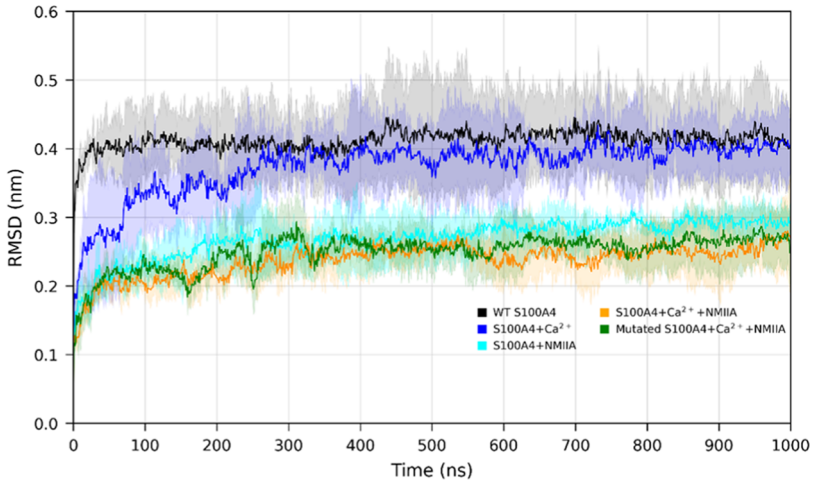

Figure 3. Average RMSD values of C_α atoms for all S100A4 proteins studied. WT S100A4, S100A4 bound to Ca^{2+}, S100A4 bound to NMIIA, S100A4 bound to Ca^{2+} and NMIIA, and mutated S100A4 bound to Ca^{2+} and NMIIA are colored as black, blue, cyan, orange, and green, respectively. Thick lines represent the averages, while shaded areas represent the standard deviations calculated from three simulations.

stability of the simulations was evaluated based on the average RMSD and RMSF from three replica 1 μs simulations. Superposition of starting structures and MD-derived structures represented by the average structures of equilibrated trajectories are given in Figure 2A–E. The RMSD of C_α atoms of WT S100A4, S100A4 bound to Ca^{2+}, S100A4 bound to NMIIA, S100A4 bound to Ca^{2+} and NMIIA, and mutated S100A4 bound to Ca^{2+} and NMIIA are 0.3, 0.3, 0.2, 0.1, and 0.2 nm, respectively.

The RMSDs of WT S100A4 (Ca^{2+} free-S100A4) and S100A4 bound to Ca^{2+} stabilize around 0.4 nm (Figure 3 black and blue lines), while for NMIIA-bound S100A4 structures, RMSDs are between 0.2 and 0.3 nm, which are lower than those of WT S100A4 and S100A4 bound to Ca^{2+}, suggesting that NMIIA binding stabilizes the S100A4 protein (Figure 3 cyan and orange lines). The RMSDs of individual trajectories are given in Figure S1 and the RMSD values of each helix from individual trajectories are given in Figures S2–S5. The RMSD of helix 1 in WT S100A4 is approximately 0.3 nm, while it is around 0.1 nm for the rest of structures, indicating that Ca^{2+} is binding to helix 1 (Figure S2). Helix 2 in NMIIA-bound structures has an RMSD of approximately 0.1 nm, and it is more stable than WT S100A4 and S100A4 bound to Ca^{2+} (Figure S3). However, helix 3 in S100A4 bound to Ca^{2+} undergoes large conformational changes compared to WT S100A4. In addition, helices 3 and 4 in chain B of NMIIA bound three structures are more stable than chain A of those structures (Figures S4 and S5). These RMSD results show that interaction between S100A4 and NMIIA stabilizes the helices 3 and 4 of chain B of S100A4 protein and chain A has a considerably less effect due to the asymmetric binding mode of NMIIA, while Ca^{2+} binding causes large conformational changes on S100A4.[31−35]

https://doi.org/10.1021/acs.jpcb.1c02096
J. Phys. Chem. B 2021, 125, 10059−10071

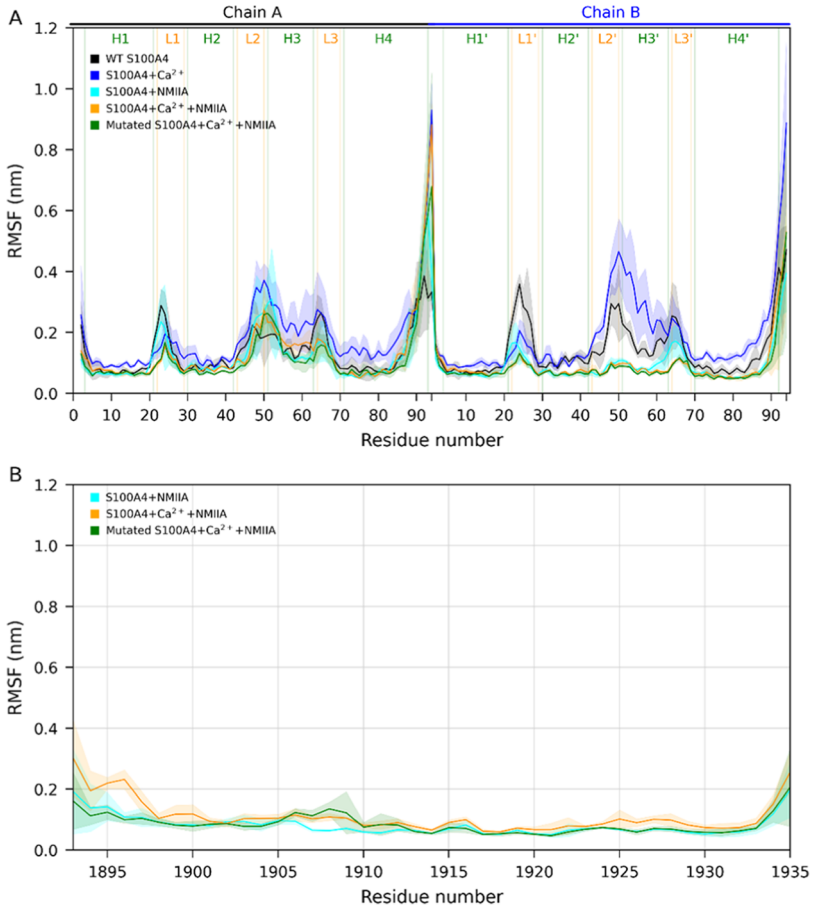

Figure 4. RMSFs of C_α atoms from the last 500 ns of the trajectories. (A) Average RMSFs of C_α atoms for all S100A4 proteins studied. (B) Average RMSFs of C_α atoms for NMIIA. WT S100A4, S100A4 bound to Ca^{2+}, S100A4 bound to NMIIA, S100A4 bound to Ca^{2+} and NMIIA, and mutated S100A4 bound to Ca^{2+} and NMIIA are colored as black, blue, cyan, orange, and green, respectively. Thick lines represent the averages, while shaded areas represent the standard deviations calculated from three simulations.

We compared the calculated and measured RMSF values of WT S100A4 (1m31[34]) and S100A4 bound to Ca^{2+} and NMIIA complex (2lnk[42]). The calculated and measured RMSFs were found to be consistent with each other as seen from Figure S6. Figure 4 represents the average RMSFs from replicate simulations of all systems studied, while RMSFs from individual trajectories are given in Figure S7. Low RMSF values are observed for NMIIA-bound structures, while the L2-H3-L3-H4 and L2′-H3′-L3′-H4′ regions of S100A4 bound to Ca^{2+} exhibit high RMSF compared to the other systems (Figure 4A). Although the presence of NMIIA seems to have an important effect on the overall conformational stability of S100A4, Ca^{2+} binding leads to the overall conformational flexibility of S100A4. Moreover, asymmetric dynamics between the L2-H3-L3-H4 and L3′-H3′-L3′-H4′ regions were observed due to the asymmetric binding of NMIIA to S100A4 for three NMIIA bound S100A4 structures. It is interesting that the binding of both Ca^{2+} and NMIIA to S100A4 stabilizes the L1 and L3 regions more as compared to NMIIA binding to Ca^{2+} free-S100A4, suggesting that Ca^{2+} mediate the interactions between NMIIA and S100A4. To investigate the effect of Ca^{2+} and mutants on NMIIA dynamics, we plotted the RMSF of C_α atoms of NMIIA (Figure 4B). We observed Ca^{2+} binding to S100A4 and/or mutations had no significant effect on the flexibility of NMIIA.

Solvent-Accessible Surface Area (SASA). To investigate the level of exposure of the residues to water molecules in the S100A4 protein, we calculated both hydrophobic solvent-accessible surface area (SASA) as a function of simulation time (Figure S8) and hydrophobic SASA per residue from individual trajectories (Figure S9). SASA of WT S100A4 is around 48 nm^2, but it has increased to approximately 50 nm^2 for S100A4 bound to Ca^{2+} and 60 nm^2 for NMIIA bound S100A4 structures (Figure S8). The average SASA per residue from replicate simulations is plotted in Figure 5A. The average SASA shows that the loops and N- and C-terminal regions of chains make important contributions to the hydrophobic SASA formation in S100A4 structures. To quantify the individual residue contribution to the SASA, we computed hydrophobic ΔSASA, which is obtained by subtracting the SASA of WT S100A4 from the SASA of the other S100A4 structures, $\Delta SASA = SASA(S100A4 + X) - SASA(WT\ S100A4)$ (Figure 5B). As shown in Figure 5B, contributions greater than 0.3 nm^2 to the SASA of S100A4 bound to Ca^{2+} come from Phe27 in L1, Lys31 in H2, Thr50 in L2, Met85 and Phe93 in H4, and Met84, Met85, and Phe89 in H4′. As for NMIIA-bound S100A4 structures, those contributions come from Phe27 in L1, Lys31 in H2, Lys48 in L2, Leu58 in H3, Met85, Phe93, and Pro94 in H4, Lys31 in H2′, Leu46 and Thr50 in L2′, Leu58 in H3′, and Val77, Met84, Met85, Phe89, Phe90, Phe93, and Pro94 in H4′. The ΔSASA results show that L2, H3, and H4 in chain A and L2′, H3′, and H4′ in chain B make the highest contributions to the formation of hydrophobic

https://doi.org/10.1021/acs.jpcb.1c02096
J. Phys. Chem. B 2021, 125, 10059−10071

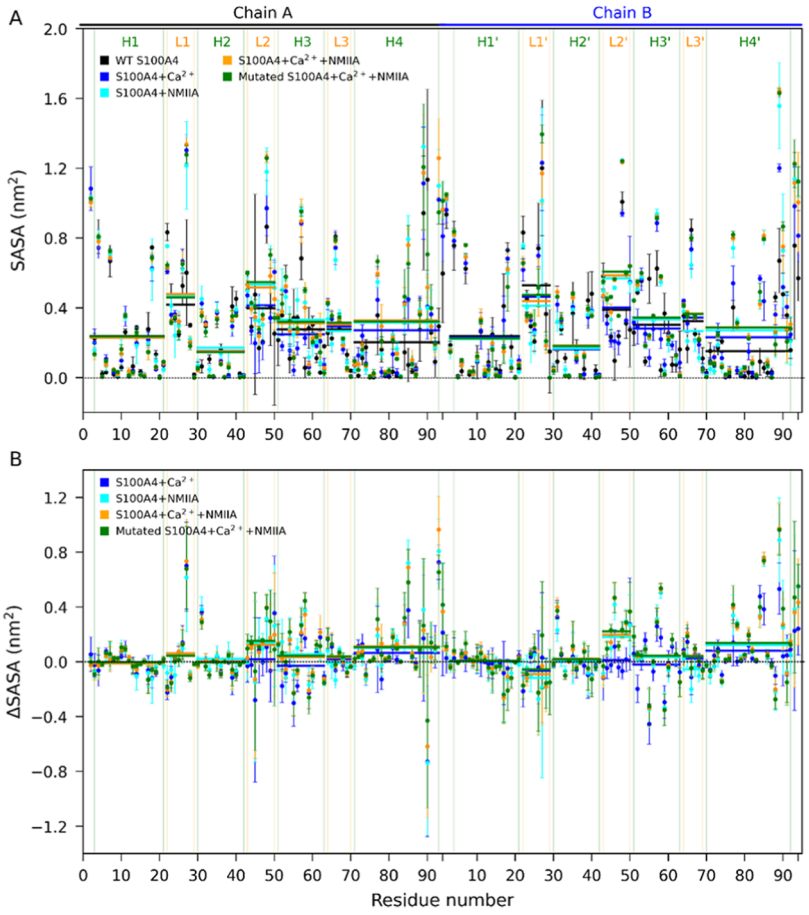

Figure 5. SASA values of S100A4 structures as a function of the residue number from the last 500 ns of the trajectories. (A) Average SASA per residue. (B) SASA difference per residue. WT S100A4, S100A4 bound to Ca^{2+}, S100A4 bound to NMIIA, S100A4 bound to Ca^{2+} and NMIIA, and mutated S100A4 bound to Ca^{2+} and NMIIA are colored as black, blue, cyan, orange, and green, respectively. Thick lines show average values, while bars represent the standard deviations calculated from three simulations.

SASA in S100A4 systems as reported by previous experimental studies.[31−35]

Conformational Entropy. Conformational entropy S of backbone atoms for all of the systems studied was calculated using the quasiharmonic approximation.[67,68] The average S is 3960 ± 64, 4428 ± 483, 3439 ± 145, 3402 ± 57, and 3708 ± 124 J/(mol K) for WT S100A4, S100A4 bound to Ca^{2+}, S100A4 bound to NMIIA, S100A4 bound to Ca^{2+} and NMIIA, and mutated S100A4 bound to Ca^{2+} and NMIIA, respectively. To investigate the effect of Ca^{2+}, mutations, and NMIIA on the entropy of S100A4, we calculated ΔS by subtracting WT S100A4 from the S of other four S100A4 structures. The obtained ΔS values are 468, −521, −559, and −720 J/(mol K) for S100A4 bound to Ca^{2+}, S100A4 bound to NMIIA, S100A4 bound to Ca^{2+} and NMIIA, and mutated S100A4 bound to Ca^{2+} and NMIIA, respectively. The calculated entropy difference (ΔS = −468 J/(mol K)) between WT S100A4 and S100A4 bound to Ca^{2+} is consistent with the value of Duelli et al. (−600 J/(mol K)).[45] The contribution to the stability ($T\Delta S$) of S100A4 of the structures at 300 K are approximately 140 314, −156 319, −167 556, and −216 025 J/mol for S100A4 bound to Ca^{2+}, S100A4 bound to NMIIA, S100A4 bound to Ca^{2+} and NMIIA, and mutated S100A4 bound to Ca^{2+} and NMIIA, respectively, indicating that Ca^{2+} binding leads to the activation of S100A4, thus leading conformational changes, while mutants have decreased the dynamic motions of S100A4.

Moreover, the conformational entropy S was calculated as a function of the residue number, as depicted in Figure 6A. The loops, H3, H3′, and C-terminal of the proteins have relatively large values. To investigate residue contributions, we calculated the conformational entropy difference as a function of the residue number, $\Delta S = S(\text{S100A4} + X) - S(\text{WT S100A4})$, as given in Figure 6B. The residues 21−25 in L1 and 63−67 in L3 for chain A and residues 21−26 in the L3′ region of S100A4 + Ca^{2+} have negative conformational entropy values, indicating that an unfavorable entropic contribution to the free energy. However, the other residues of S100A4 + Ca^{2+} have positive values, suggesting that S100A4 is activated upon Ca^{2+} binding and the highest entropic contribution to the free energy comes from almost all regions except L1 and L3 loops in chain A and L1′ in chain B. Moreover, loops in NMIIA-bound structures cause the unfavorable (negative) entropic contribution to the free energy of calcium and/or NMIIA binding. These results show that Ca^{2+}-bound S100A4 is the most favorable state because positive conformational entropy results in lower free energy.

Principal Component Analysis (PCA). For a more detailed investigation of the structural changes and the dynamics in S100A4 systems, we performed principal component analysis (PCA) in two ways: first on the covariance

https://doi.org/10.1021/acs.jpcb.1c02096
J. Phys. Chem. B 2021, 125, 10059−10071

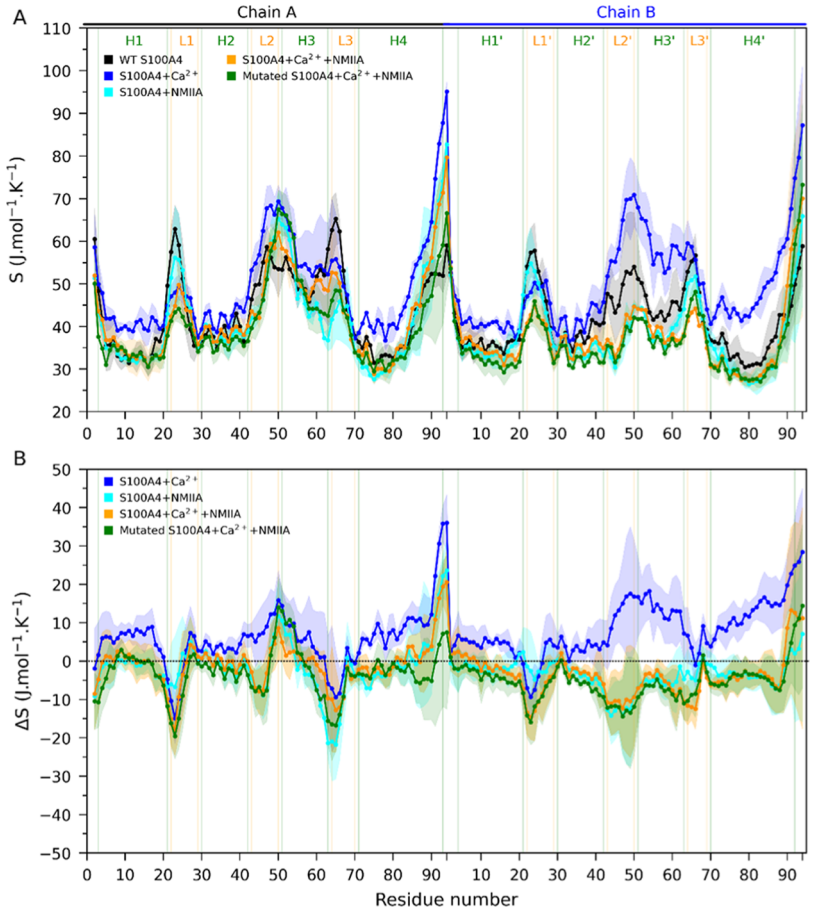

Figure 6. Conformational entropy as a function of the residue number from the last 500 ns of the trajectories. (A) Average conformational entropy S per residue. (B) Entropy difference ΔS per residue. WT S100A4, S100A4 bound to Ca^{2+}, S100A4 bound to NMIIA, S100A4 bound to Ca^{2+} and NMIIA, and mutated S100A4 bound to Ca^{2+} and NMIIA are colored as black, blue, cyan, orange, and green, respectively. Thick lines represent the averages, while shaded areas represent the standard deviations calculated from three simulations.

matrix of the joint set of trajectories and second on the last 500 ns of each MD trajectory individually.

Performing PCA on a joint set of trajectories provides a mixed view of the variance structure between trajectories and within trajectories and allows assessment of the relative importance of the two sources by plotting the projections and marking the average structures.[69,70] The joint covariance matrix was determined after fitting all structures to a common reference. We also included all structures obtained by swapping the two chains in the dimers, as both chains are thermodynamically indistinguishable and any asymmetry should be considered equally likely for the other permutation. The covariance matrix had a trace of 10.67 nm^2 and the first three eigenvectors captured 63, 8, and 7% of the total variance, respectively. The first two components were rotated using a varimax rotation, resulting in factors with a simpler structure, which makes them more interpretable. The main results from this factor analysis are given in Figure 7, which shows the scores of all frames from all trajectories on the factors, together with markers indicating starting points and average structures from the last 500 ns of each trajectory. The scores are normalized, such that the distance between any two structures in the configurational space approximately equals the RMSD between them. The inset shows the structures colored according to the loadings for the first two factors. From the figure, each group of trajectories appears to have a specific region in conformational space associated with it, suggesting that the first two eigenvectors are indeed dominated by the between group variances. Together, the scores trace out a region that shows the configurational changes associated with the functional states of S100A4: the blue markers indicate the region sampled by simulations started from the apo state NMR structure 1m31, which appear to remain separated from the other regions over factor 1, corresponding to a remodeling of the calcium-binding region and associated changes in the loop connecting H2 and H3. The apo structure obtained by removal of calcium from PDB ID: 2q91 (magenta) ends up sampling the "low" end of factor 2 but does not cross to the other side of factor 1. This suggests that there is a barrier between the two regions, pertaining to the rearrangement of calcium-binding sites that would require longer time scales to cross. The binding of calcium (orange) causes a shift "up" over factor 2, involving a change in the configuration of the H3 N-terminal region. It is worth noting that the differences between the starting structure and the final structures are largest for simulations starting from the calcium-bound state, relaxing along the observed factor 2. Finally, binding of NMIIA causes a further conformational change to the up end on factor 2.

The points in green mark the regions sampled when calcium is removed from the NMIIA-bound structure. Although not a physiologically known state, as calcium binding is a prerequisite for binding of NMIIA, it may play a role as intermediate in unbinding, especially when calcium levels drop, and the solvent-exposed binding sites could deplete. It is

https://doi.org/10.1021/acs.jpcb.1c02096
J. Phys. Chem. B 2021, 125, 10059−10071

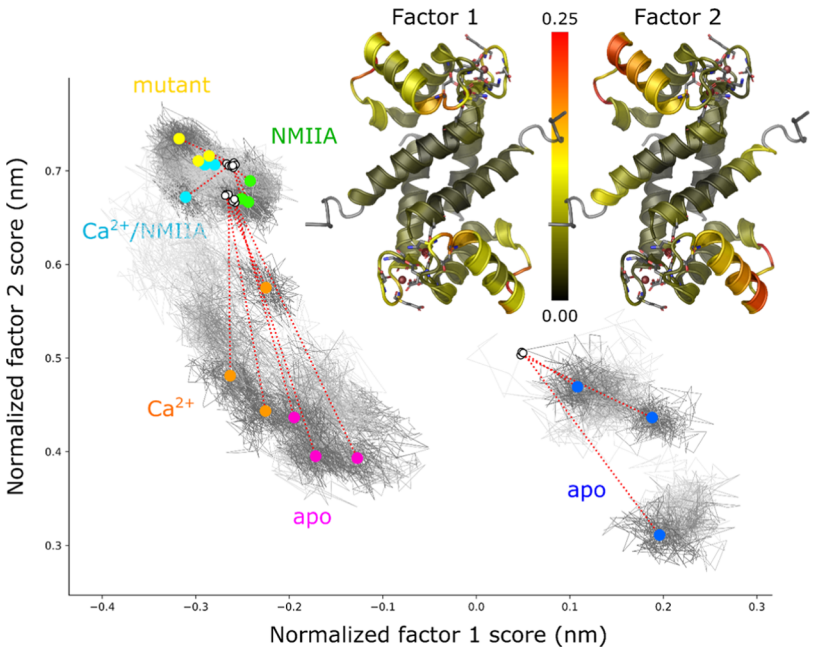

Figure 7. Results from factor analysis on joint trajectories. The plot shows the projections of all 18 trajectories onto the first two factors obtained from the joint covariance matrix, while the insets show the protein structure (PDB ID: 2q91) colored according to the loadings of factors 1 and 2. The scores are normalized, such that the distance between points corresponds to the RMSD between the structures. In the plot, trajectories are colored over time from light gray to dark gray, starting structures are indicated with white circles with a black outline, and the average structures from the last 500 ns of each trajectory are indicated with colored points, of which the colors correspond to those in Figure 8. Red dotted lines are used to connect starting points and end points. It is clear that removal of NMIIA is associated with a conformational change on factor 2, which, from the inset, appears associated with changes in the calcium-binding region and the opposite end of helix 3. Factor 1 appears to capture a motion of the N-terminal region of helix 3 and seems associated with the difference between the calcium-bound forms and the apo form (blue). Removal of calcium from the calcium-bound structure (magenta) causes a further shift on factor 2, but does not shift over factor 1 to the original apo form.

evident that this has little effect on the structure of the complex on the time scales sampled, and thus, no conclusions can be drawn yet as to a possible responsiveness to a drop in the calcium concentration.

The joint PCA clearly shows that each system has a characteristic region in configurational space associated with it. It is likely that each region also has its own characteristic motions, as different states have quite different constraints imposed by the binding of Ca^{2+} and NMIIA. To assess these differences in dynamics per system, we performed PCA on covariance matrices obtained from the last 500 ns of each individual trajectory, for the dimer and for the two chains separately. The traces of covariance matrices themselves allow a first assessment of the total motility of each dimer and how this relates to the motility of individual subunits. Figure S10 shows a scatterplot of the motility of dimers against the motility from the subunits and their sums. The WT complexes with Ca^{2+} and NMIIA are characterized by strongly reduced motility, with the total motility (2.52, 2.51, and 4.16 nm^2) being approximately equal to the sum of that of the subunits (2.05, 2.04, and 3.35 nm^2), showing that relative motions between the subunits are diminished. The mutant (2.83, 4.17, and 5.83 nm^2) and the NMIIA-bound form without calcium (4.12, 5.63, and 6.19 nm^2) appear more mobile, but still with little relative motion of the chains, due to the fixation by the peptide. Interestingly, the apo form of the protein (5.22, 6.18, and 6.89 nm^2) appears less dynamic than either the calcium-bound form (6.65, 6.92, and 10.64 nm^2) or the structure from which calcium was removed (6.59, 7.52, and 8.44 nm^2). In these systems, there are also considerably more dynamics between the chains. These findings suggest that the coordination of calcium-binding sites releases other parts of the protein causing an overall increase in motility. This is expected to be related to the shift over factor 1 as shown in Figure 7, which corresponds to a coupling between the calcium-binding sites and the dynamics of the loop connecting H2 and H3.

Figure 8 shows the first eigenvector for each system, determined and drawn using a previously developed PCA module for PyMOL.[69,70] These results show that in the individual systems the first eigenvector captures between 10 and 30% of the total motility, suggesting that there is little concerted motion. However, it can also be seen that the contribution of the first eigenvector is more important in the systems with more dynamics, notably the Ca^{2+}-bound form, where the first eigenvector captures between 20 and 30% of the total variance in the system. The second eigenvectors in this system contribute another 10−16% (data not shown). The figures also show that most of the motion pertains either to calcium-binding sites or to the loop connecting H2 and H3, consolidating the view that the binding of calcium remodels the calcium-binding site and destabilizes that loop, causing an increase in overall dynamics.

Linear Mutual Information (LMI). The results from the previous sections suggest that Ca^{2+} leads to enhanced dynamics as compared to the wild-type S100A4. However, the effect of Ca^{2+} binding on NMIIA-bound states is not yet clear. To further characterize this relation, we decided to determine linear mutual information (LMI) of residue fluctuations.[71] In this case, if fluctuations of two residues are correlated linearly, the pairwise LMI is 1, and only if they are completely independent, the pairwise LMI is 0. We calculated

https://doi.org/10.1021/acs.jpcb.1c02096
J. Phys. Chem. B 2021, 125, 10059−10071

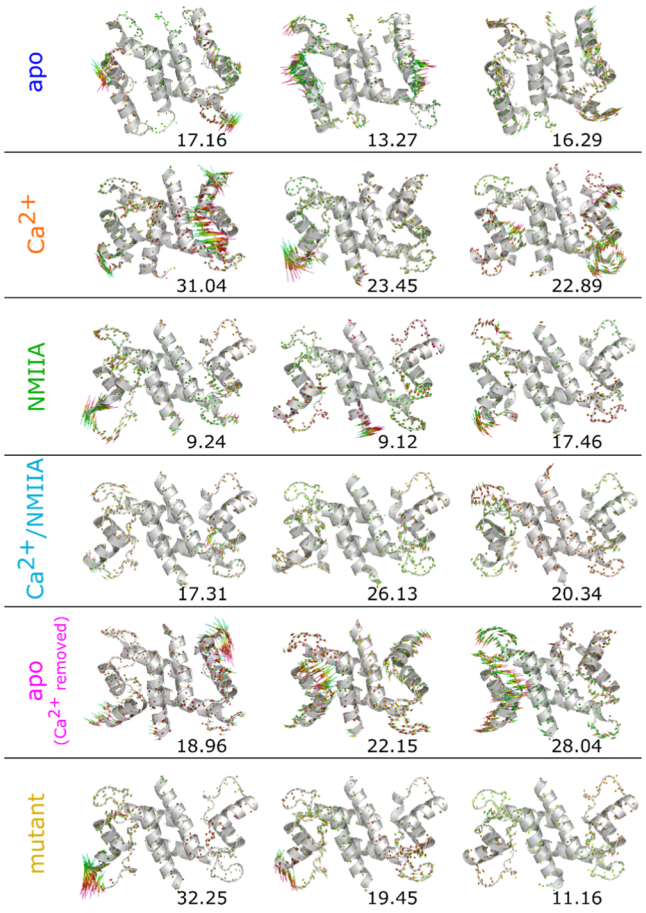

Figure 8. First principal component from the last 500 ns for each trajectory. For each system, the vector of loadings is shown as per particle bars superposed on average structures with a thin line marking the extent of projections and a thicker tube marking the middle 50% of projections. The bars are colored from cyan to magenta to allow the assessment of directional correlation. The numbers indicate the percentage of the total positional variance associated with the first eigenvector.

the LMI using the g_correlation tool[71] of GROMACS and the correlationplus (https://github.com/tekpinar/correlationplus) python package. As shown from Figure 9A,B, S100A4 shows increased correlations when bound to Ca^{2+}. It is clear that Ca^{2+} binding leads to the increase of linear correlations but NMIIA and mutations reduce those correlations. LMI also reveals the opposing roles of Ca^{2+} and NMIIA: if only NMIIA is bound, the correlations are reduced significantly and LMI maps are quite similar to WT S100A4 maps (Figure 9A vs C). When Ca^{2+} is added to the NMIIA-bound state, it increases the correlations and the map in Figure 9D is more similar to Figure 9B. As a result, we observe that while Ca^{2+} increases LMI correlations, NMIIA reduces them. Therefore, Ca^{2+} and NMIIA have competing roles in the dynamics of S100A4.

Furthermore, it was observed that the degree of correlations of the mutated S100A4 bound to Ca^{2+} and NMIIA are lower compared with those of S100A4 bound to Ca^{2+} and NMIIA. This shows that mutations that were done to avoid the interunit disulfide bond formation prevent the dynamical correlations of S100A4 as well, suggesting that these residues play an important role in the conformational dynamics of S100A4. Moreover, we checked the inter- and intrachain linear correlations for all of the systems studied in replica trajectory sets (Figures S11 and S12). It seems that the most contribution to linear correlations comes from intrachain correlations, while strong interchain correlations between chains of S100A4 were not observed. Interestingly, in all S100A4 structures studied, strong intrachain correlations (higher than 0.7) were observed between the residues 69−71 of loop 3 (Figures S11 and S12).

To understand the impact of Ca^{2+} and mutants on the interaction of S100A4 with NMIIA, we computed interchain correlations between S100A4 and NMIIA (Figure 10A−D). We observed that strongest correlations occur between the residues 1927−1930 of NMIIA and residues 45−50 of loop 2 in the chain B of S100A4. The correlation degrees between those residues in S100A4 bound to Ca^{2+} and NMIIA are stronger than those of Ca^{2+} free-S100A4 bound to NMIIA and the mutated S100A4 bound to Ca^{2+} and NMIIA. It is clear that Ca^{2+} binding to S100A4 mediates the interchain correlations between NMIIA and S100A4, but mutations inhibit those correlations. Moreover, we observed strong intracorrelations between the residues 69−71 of loop 3 in all S100A4 proteins, especially in the absence of Ca^{2+}.

CONCLUSIONS

In this work, we show that WT S100A4 is in an inactive state, but upon Ca^{2+} binding, S100A4 undergoes a conformational change as reported by many experimental studies.[31−35] However, NMIIA induces asymmetric dynamics on S100A4 due to the asymmetric binding of NMIIA to S100A4. For both S100A4 bound to NMIIA and WT S100A4 simulations, both intrachain and interchain correlations are very low. However, Ca^{2+} binding has increased the dynamics of S100A4 and NMIIA, accordingly the interactions of S100A4 with NMIIA as well, indicating that S100A4 interaction with NMIIA is dependent on Ca^{2+} binding. We also identified some key residues (residues 1927−1930 of NMIIA and residues 45−50 of loop 2 in the chain B of S100A4) that are involved in the strong interchain correlations between NMIIA and S100A4 in the presence of Ca^{2+}. On the other hand, NMIIA behaves like a competitor of Ca^{2+} in terms of the LMI maps and it reduces the correlations gained by Ca^{2+} binding. Moreover, mutations made to avoid disulfide bond formation reduce the correlations to a lower level, thus leading to the decrease in binding capability of S100A4 to NMIIA,[52] almost to the point where Ca^{2+} is not bound. Additionally, for mutated S100A4 bound to Ca^{2+} and NMIIA, the conformational entropy (average S) and variance results of PCA are lower than those of other structures, indicating that preventing disulfide bond formation decreases the flexibility of S100A4; thus, certain mutations play an important regulator role in the structural dynamics of S100A4. In conclusion, the binding of Ca^{2+} and NMIIA to S100A4 regulate competitively the dynamics of S1004 in terms of RMSF, conformational entropy, PCA, and LMI results, while mutations reduce them.

In summary, we have shown that Ca^{2+} and NMIIA modulate competitively the dynamics of S100A4. As Ca^{2+} binding to S100A4 increases, the dynamics of S100A4 and NMIIA binding decreases; Ca^{2+} and NMIIA binding at the same time reduce the Ca^{2+}-induced enhanced dynamics. Moreover, Ca^{2+} binding modulates the dynamics of S100A4 and NMIIA by enabling enhanced dynamics, while mutations made to prevent disulfide bond formation lead to the decreased dynamics of S100A4 and NMIIA. This finding is in line with the 2 orders of magnitude lower affinity between the mutated S100A4 bound

https://doi.org/10.1021/acs.jpcb.1c02096
J. Phys. Chem. B 2021, 125, 10059−10071

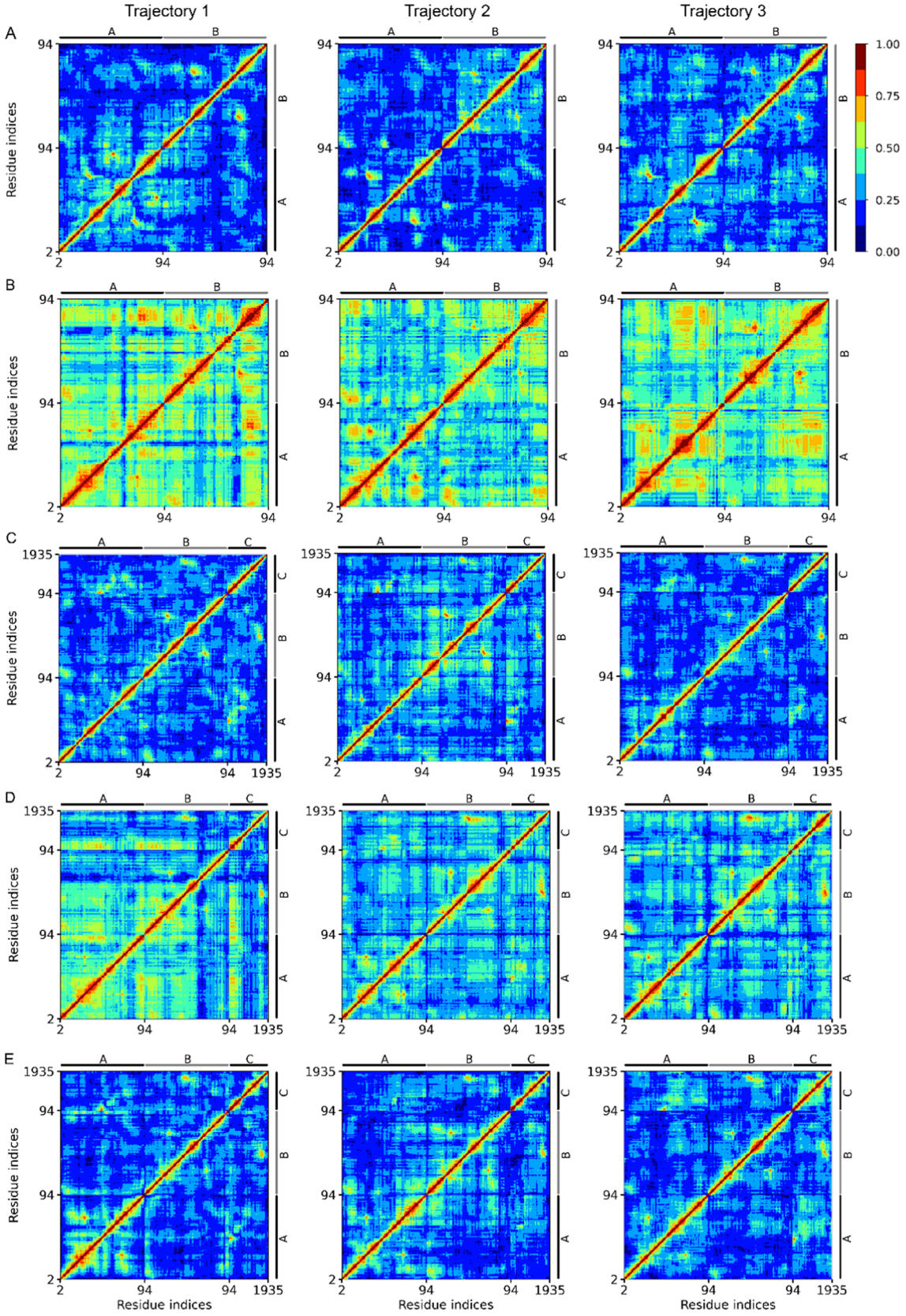

Figure 9. LMI maps from the last 500 ns of the trajectories. LMI varies from 0 to 1. LMI value 1 defines complete linear correlations, (shown in red), while 0 means no correlation (shown in blue). (A) WT S100A4. (B) S100A4 bound to Ca^{2+}. (C) S100A4 bound to NMIIA. (D) S100A4 bound to Ca^{2+} and NMIIA. (E) Mutated S100A4 bound to Ca^{2+} and NMIIA.

to Ca^{2+} and NMIIA compared to that of the unmutated structure (S100A4 bound to Ca^{2+} and NMIIA).[52] These results provide novel insights into better understanding the role of Ca^{2+}, NMIIA and certain, structure stabilizing

https://doi.org/10.1021/acs.jpcb.1c02096
J. Phys. Chem. B 2021, 125, 10059−10071

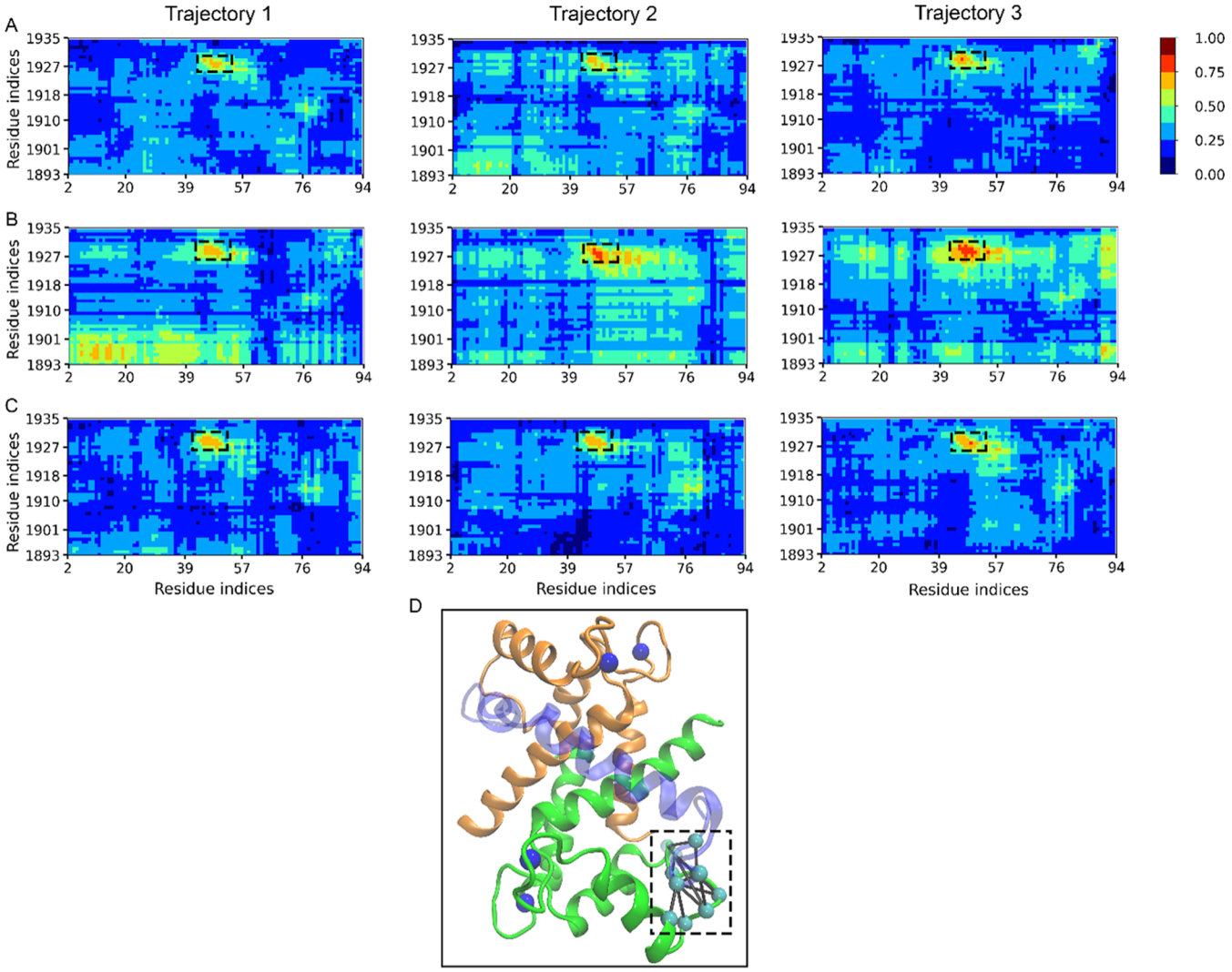

Figure 10. Interchain LMI maps calculated from the last 500 ns of the trajectories. LMI varies from 0 to 1. Here, 1 defines complete linear correlations (shown in red), while 0 means no correlation (shown in blue). (A) S100A4 bound to NMIIA. (B) S100A4 bound to Ca^{2+} and NMIIA. (C) Mutated S100A4 bound to Ca^{2+} and NMIIA. (D) S100A4 bound to Ca^{2+} and NMIIA given in New Cartoon representation. Black dashed squares highlight interdomain LMI comprised of residues 1927−1930 in NMIIA and residues 45−50 in the chain B of S100A4.

mutations on the dynamics of S100A4, and they suggest that shifting Ca^{2+} and NMIIA equilibrium may be an alternative strategy for the design of new drugs that inhibit S100A4 activity and/or disrupt the interaction of S100A4 with NMIIA.

■ ASSOCIATED CONTENT

Supporting Information

The Supporting Information is available free of charge at https://pubs.acs.org/doi/10.1021/acs.jpcb.1c02096.

Molecular dynamics system compositions for all systems used in this study; RMSDs of C_α atoms for all S100A4 proteins studied; C_α RMSDs of helix 1−4 in structures studied; the calculated and measured RMSFs of C_α atoms; RMSFs of C_α atoms for all S100A4 proteins studied; hydrophobic SASA of structures studied against simulation time; hydrophobic SASA of structures studied per residue; overall and within subunit motility in all trajectories; intra-LMI maps of chain A in S100A4 structures from the last 500 ns of the trajectories; and intra-LMI maps of chain B in S100A4 structures from the last 500 ns of the trajectories (PDF)

■ AUTHOR INFORMATION

Corresponding Author

Ahmet Yildirim − *Department of Physics, Siirt University, Siirt 56100, Turkey;* orcid.org/0000-0003-1495-0288; Email: ahmedoyildirim@siirt.edu.tr

Authors

Mustafa Tekpinar − *Unit of Structural Dynamics of Biological Macromolecules, Pasteur Institute, UMR 3528 CNRS, 75015 Paris, France*

Tsjerk A. Wassenaar − *Groningen Biomolecular Sciences and Biotechnology Institute and Zernike Institute for Advanced Materials, University of Groningen, 9747 AG Groningen, The Netherlands; Data Science for Life Sciences, Hanze University of Applied Sciences, 9747 AS Groningen, The Netherlands*

Complete contact information is available at: https://pubs.acs.org/10.1021/acs.jpcb.1c02096

https://doi.org/10.1021/acs.jpcb.1c02096
J. Phys. Chem. B 2021, 125, 10059−10071

Author Contributions

The manuscript was written through the contributions of all authors. All authors have given approval to the final version of the manuscript.

Notes

The authors declare no competing financial interest.

■ ACKNOWLEDGMENTS

All molecular dynamics simulations reported in this paper were performed at TUBITAK (Scientific and Technical Research Council of Turkey) ULAKBIM (National Academic Information Center), High Performance and Grid Computing Center (TRUBA Resources). The authors would like to thank TUBITAK for providing us these computational resources and service.

■ ABBREVIATIONS USED

MD, molecular dynamics; NMIIA, nonmuscle myosin IIA; RMSD, root-mean-square deviations; RMSF, root-mean-square fluctuations; SASA, solvent-accessible surface area; PCA, principal component analysis; LMI, linear mutual information

■ REFERENCES

(1) Carafoli, E. Calcium Signaling: A Tale for All Seasons. *Proc. Natl. Acad. Sci. U.S.A.* **2002**, *99*, 1115−1122.
(2) Berridge, M. J.; Lipp, P.; Bootman, M. D. The Versatility and Universality of Calcium Signalling. *Nat. Rev. Mol. Cell Biol.* **2000**, *1*, 11−21.
(3) Parekh, A. B. Decoding Cytosolic Ca2+ Oscillations. *Trends Biochem. Sci.* **2011**, *36*, 78−87.
(4) Nelson, M. R.; Chazin, W. J. An Interaction-Based Analysis of Calcium-Induced Conformational Changes in Ca2+ Sensor Proteins. *Protein Sci.* **1998**, *7*, 270−282.
(5) Schneider, M.; Kostin, S.; Strøm, C. C.; Aplin, M.; Lyngbæk, S.; Theilade, J.; Grigorian, M.; Andersen, C. B.; Lukanidin, E.; Lerche Hansen, J.; et al. S100A4 Is Upregulated in Injured Myocardium and Promotes Growth and Survival of Cardiac Myocytes. *Cardiovasc. Res.* **2007**, *75*, 40−50.
(6) Ambartsumian, N.; Klingelhöfer, J.; Grigorian, M.; Christensen, C.; Kriajevska, M.; Tulchinsky, E.; Georgiev, G.; Berezin, V.; Bock, E.; Rygaard, J.; et al. The Metastasis-Associated Mts1 (S100A4) Protein Could Act as an Angiogenic Factor. *Oncogene* **2001**, *20*, 4685−4695.
(7) Boye, K.; Maelandsmo, G. M. S100A4 and Metastasis: A Small Actor Playing Many Roles. *Am. J. Pathol.* **2010**, *176*, 528−535.
(8) Helfman, D. M.; Kim, E. J.; Lukanidin, E.; Grigorian, M. The Metastasis Associated Protein S100A4: Role in Tumour Progression and Metastasis. *Br. J. Cancer* **2005**, *92*, 1955−1958.
(9) Mazzucchelli, L. Protein S100A4: Too Long Overlooked by Pathologists? *Am. J. Pathol.* **2002**, *160*, 7−13.
(10) Serrano, A.; Apolloni, S.; Rossi, S.; Lattante, S.; Sabatelli, M.; Peric, M.; Andjus, P.; Michetti, F.; Carrì, M. T.; Cozzolino, M.; et al. The S100A4 Transcriptional Inhibitor Niclosamide Reduces Pro-Inflammatory and Migratory Phenotypes of Microglia: Implications for Amyotrophic Lateral Sclerosis. *Cells* **2019**, *8*, No. 1261.
(11) Kim, E. J.; Helfman, D. M. Characterization of the Metastasis-Associated Protein, S100A4 Roles of Calcium Binding and Dimerization in Cellular Localization and Interaction with Myosin. *J. Biol. Chem.* **2003**, *278*, 30063−30073.
(12) Li, Z. H.; Bresnick, A. R. The S100A4 Metastasis Factor Regulates Cellular Motility via a Direct Interaction with Myosin-IIA. *Cancer Res.* **2006**, *66*, 5173−5180.
(13) Grigorian, M.; Ambartsumian, N.; Lykkesfeldt, A. E.; Bastholm, L.; Elling, F.; Georgiev, G.; Lukanidin, E. Effect of Mts1 (S100A4) Expression on the Progression of Human Breast Cancer Cells. *Int. J. Cancer* **1996**, *67*, 831−841.
(14) Davies, B. R.; Davies, M. P.; Gibbs, F. E.; Barraclough, R.; Rudland, P. S. Induction of the Metastatic Phenotype by Transfection of a Benign Rat Mammary Epithelial Cell Line with the Gene for P9Ka, a Rat Calcium-Binding Protein, but Not with the Oncogene EJ-Ras-1. *Oncogene* **1993**, *8*, 999−1008.
(15) Bresnick, A. R. S100 Proteins as Therapeutic Targets. *Biophys. Rev.* **2018**, *10*, 1617−1629.
(16) Rudland, P. S.; Platt-Higgins, A.; Renshaw, C.; West, C. R.; Winstanley, J. H. R.; Robertson, L.; Barraclough, R. Prognostic Significance of the Metastasis-Inducing Protein S100A4 (P9Ka) in Human Breast Cancer. *Cancer Res.* **2000**, *60*, 1595−1603.
(17) Cho, Y. G.; Nam, S. W.; Kim, T. Y.; Kim, Y. S.; Kim, C. J.; Park, J. Y.; Lee, J. H.; Kim, H. S.; Lee, J. W.; Park, C. H.; et al. Overexpression of S100A4 Is Closely Related to the Aggressiveness of Gastric Cancer. *Apmis* **2003**, *111*, 539−545.
(18) Kim, B.; Jung, S.; Kim, H.; Kwon, J. O.; Song, M. K.; Kim, M. K.; Kim, H. J.; Kim, H. H. The Role of S100A4 for Bone Metastasis in Prostate Cancer Cells. *BMC Cancer* **2021**, *21*, No. 137.
(19) Saleem, M.; Kweon, M.-H.; Johnson, J. J.; Adhami, V. M.; Elcheva, I.; Khan, N.; Hafeez, B.; Bin; Bhat, K. M. R.; Sarfaraz, S.; Reagan-Shaw, S.; et al. S100A4 Accelerates Tumorigenesis and Invasion of Human Prostate Cancer through the Transcriptional Regulation of Matrix Metalloproteinase 9. *Proc. Natl. Acad. Sci. U.S.A.* **2006**, *103*, 14825−14830.
(20) Takenaga, K.; Nakanishi, H.; Wada, K.; Suzuki, M.; Matsuzaki, O.; Matsuura, A.; Endo, H. Increased Expression of S100A4, a Metastasis-Associated Gene, in Human Colorectal Adenocarcinomas. *Clin. Cancer Res.* **1997**, *3*, 2309−2316.
(21) Komatsu, K.; Murata, K.; Kameyama, M.; Ayaki, M.; Mukai, M.; Ishiguro, S.; Miyoshi, J.; Tatsuta, M.; Inoue, M.; Nakamura, H. Expression of S100A6 and S100A4 in Matched Samples of Human Colorectal Mucosa, Primary Colorectal Adenocarcinomas and Liver Metastases. *Oncology* **2002**, *63*, 192−200.
(22) Grum-Schwensen, B.; Klingelhöfer, J.; Grigorian, M.; Almholt, K.; Nielsen, B. S.; Lukanidin, E.; Ambartsumian, N. Lung Metastasis Fails in MMTV-PyMT Oncomice Lacking S100A4 Due to a T-Cell Deficiency in Primary Tumors. *Cancer Res.* **2010**, *70*, 936−947.
(23) Ai, K.-X.; Lu, L.-Y.; Huang, X.-Y.; Chen, W.; Zhang, H.-Z. Prognostic Significance of S100A4 and Vascular Endothelial Growth Factor Expression in Pancreatic. *World J. Gastroenterol.* **2008**, *14*, No. 1931.
(24) Nakamura, T.; Ajiki, T.; Murao, S.; Kamigaki, T.; Maeda, S.; Ku, Y.; Kuroda, Y. Prognostic Significance of S100A4 Expression in Gallbladder Cancer. *Int. J. Oncol.* **2002**, *20*, 937−941.
(25) Kikuchi, N.; Horiuchi, A.; Osada, R.; Imai, T.; Wang, C.; Chen, X.; Konishi, I. Nuclear Expression of S100A4 Is Associated with Aggressive Behavior of Epithelial Ovarian Carcinoma: An Important Autocrine/Paracrine Factor in Tumor Progression. *Cancer Sci.* **2006**, *97*, 1061−1069.
(26) Davies, B. R.; O'Donnell, M.; Durkan, G. C.; Rudland, P. S.; Barraclough, R.; Neal, D. E.; Kilian Mellon, J. Expression of S100A4 Protein Is Associated with Metastasis and Reduced Survival in Human Bladder. *J. Pathol.* **2002**, *196*, 292−299.
(27) Ninomiya, I.; Ohta, T.; Fushida, S.; Endo, Y.; Hashimoto, T.; Yagi, M.; Fujimura, T.; Nishimura, G.; Tani, T.; Shimizu, K.; et al. Increased Expression of S100A4 and Its Prognostic Significance in Esophageal Squamous Cell Carcinoma. *Int. J. Oncol.* **2001**, *18*, 715−720.
(28) Zou, M.; Famulski, K. S.; Parhar, R. S.; Baitei, E.; Al-Mohanna, F. A.; Farid, N. R.; Shi, Y. Microarray Analysis of Metastasis-Associated Gene Expression Profiling in a Murine Model of Thyroid Carcinoma Pulmonary Metastasis: Identification of S100A4 (Mts1) Gene Overexpression as a Poor Prognostic Marker for Thyroid Carcinoma. *J. Clin. Endocrinol. Metab.* **2004**, *89*, 6146−6154.
(29) Zimmer, D. B.; Cornwall, E. H.; Landar, A.; Song, W. The S100 Protein Family: History, Function, and Expression. *Brain Res. Bull.* **1995**, *37*, 417−429.

https://doi.org/10.1021/acs.jpcb.1c02096
J. Phys. Chem. B 2021, 125, 10059−10071

(30) Xia, C.; Braunstein, Z.; Toomey, A. C.; Zhong, J.; Rao, X. S100 Proteins as an Important Regulator of Macrophage Inflammation. *Front. Immunol.* **2018**, *8*, No. 1908.
(31) Badyal, S. K.; Basran, J.; Bhanji, N.; Kim, J. H.; Chavda, A. P.; Jung, H. S.; Craig, R.; Elliott, P. R.; Irvine, A. F.; Barsukov, I. L.; et al. Mechanism of the Ca2+-Dependent Interaction between S100A4 and Tail Fragments of Nonmuscle Myosin Heavy Chain IIA. *J. Mol. Biol.* **2011**, *405*, 1004−1026.
(32) Fei, F.; Qu, J.; Zhang, M.; Li, Y.; Zhang, S. S100A4 in Cancer Progression and Metastasis: A Systematic Review. *Oncotarget* **2017**, *8*, 73219−73239.
(33) Malashkevich, V. N.; Varney, K. M.; Garrett, S. C.; Wilder, P. T.; Knight, D.; Charpentier, T. H.; Ramagopal, U. A.; Almo, S. C.; Weber, D. J.; Bresnick, A. R. Structure of Ca2+-Bound S100A4 and Its Interaction with Peptides Derived from Nonmuscle Myosin-IIA. *Biochemistry* **2008**, *47*, 5111−5126.
(34) Vallely, K. M.; Rustandi, R. R.; Ellis, K. C.; Varlamova, O.; Bresnick, A. R.; Weber, D. J. Solution Structure of Human Mts1 (S100A4) as Determined by NMR Spectroscopy. *Biochemistry* **2002**, *41*, 12670−12680.
(35) Garrett, S. C.; Varney, K. M.; Weber, D. J.; Bresnick, A. R. S100A4, a Mediator of Metastasis. *J. Biol. Chem.* **2006**, *281*, 677−680.
(36) Donato, R.; R Cannon, B.; Sorci, G.; Riuzzi, F.; Hsu, K.; J Weber, D.; L Geczy, C. Functions of S100 Proteins. *Curr. Mol. Med.* **2012**, *13*, 24−57.
(37) Dulyaninova, N. G.; Bresnick, A. R. The Heavy Chain Has Its Day: Regulation of Myosin-II Assembly. *Bioarchitecture* **2013**, *3*, 77−85.
(38) Ford, H. L.; Silver, D. L.; Kachar, B.; Sellers, J. R.; Zain, S. B. Effect of Mts1 on the Structure and Activity of Nonmuscle Myosin II. *Biochemistry* **1997**, *36*, 16321−16327.
(39) Li, Z.-H.; Spektor, A.; Varlamova, O.; Bresnick, A. R. Mts1 Regulates the Assembly of Nonmuscle Myosin-IIA. *Biochemistry* **2003**, *42*, 14258−14266.
(40) Kriajevska, M. V.; Cardenas, M. N.; Grigorian, M. S.; Ambartsumian, N. S.; Georgiev, G. P.; Lukanidin, E. M. Non-Muscle Myosin Heavy Chain as a Possible Target for Protein Encoded by Metastasis-Related Mts-1 Gene. *J. Biol. Chem.* **1994**, *269*, 19679−19682.
(41) Bresnick, A. R.; Weber, D. J.; Zimmer, D. B. S100 Proteins in Cancer HHS Public Access. *Nat. Rev. Cancer* **2015**, *15*, 96−109.
(42) Elliott, P. R.; Irvine, A. F.; Jung, H. S.; Tozawa, K.; Pastok, M. W.; Picone, R.; Badyal, S. K.; Basran, J.; Rudland, P. S.; Barraclough, R.; et al. Asymmetric Mode of Ca 2+-S100A4 Interaction with Nonmuscle Myosin IIA Generates Nanomolar Affinity Required for Filament Remodeling. *Structure* **2012**, *20*, 654−666.
(43) Pálfy, G.; Kiss, B.; Nyitray, L.; Bodor, A. Multilevel Changes in Protein Dynamics upon Complex Formation of the Calcium-Loaded S100A4 with a Nonmuscle Myosin IIA Tail Fragment. *ChemBioChem* **2016**, *17*, 1829−1838.
(44) Dutta, K.; Cox, C. J.; Huang, H.; Basavappa, R.; Pascal, S. M. Calcium Coordination Studies of the Metastatic Mts1 Protein. *Biochemistry* **2002**, *41*, 4239−4245.
(45) Duelli, A.; Kiss, B.; Lundholm, I.; Bodor, A.; Petoukhov, M. V.; Svergun, D. I.; Nyitray, L.; Katona, G. The C-Terminal Random Coil Region Tunes the Ca2+-Binding Affinity of S100A4 through Conformational Activation. *PLoS One* **2014**, *9*, No. e97654.
(46) Zhang, S.; Wang, G.; Liu, D.; Bao, Z.; Fernig, D. G.; Rudland, P. S.; Barraclough, R. The C-Terminal Region of S100A4 Is Important for Its Metastasis-Inducing Properties. *Oncogene* **2005**, *24*, 4401−4411.
(47) Ismail, T. M.; Fernig, D. G.; Rudland, P. S.; Terry, C. J.; Wang, G.; Barraclough, R. The Basic C-Terminal Amino Acids of Calcium-Binding Protein S100A4 Promote Metastasis. *Carcinogenesis* **2008**, *29*, 2259−2266.
(48) Fritz, G. X-Ray Structural Analysis of S100 Proteins. In *Calcium-Binding Proteins and RAGE*; Methods in Molecular Biology; Springer, 2013; Vol. *963*, pp 87−97.
(49) Tsuchiya, M.; Yamaguchi, F.; Shimamoto, S.; Fujimoto, T.; Tokumitsu, H.; Tokuda, M.; Kobayashi, R. Oxidized S100A4 Inhibits the Activation of Protein Phosphatase 5 through S100A1 in MKN-45 Gastric Carcinoma Cells. *Int. J. Mol. Med.* **2014**, *34*, 1713−1719.
(50) Schrodinger, L. L. C. *The PyMOL Molecular Graphics System.*, Version 1.3r1, Scientific Research, 2010.
(51) Westbrook, J.; Feng, Z.; Jain, S.; Bhat, T. N.; Thanki, N.; Ravichandran, V.; Gilliland, G. L.; Bluhm, W.; Weissig, H.; Greer, D. S.; et al. The Protein Data Bank: Unifying the Archive. *Nucleic Acids Res.* **2002**, *30*, 245−248.
(52) Kiss, B.; Duelli, A.; Radnai, L.; Kékesi, K. A.; Katona, G.; Nyitray, L. Crystal Structure of the S100A4-Nonmuscle Myosin IIA Tail Fragment Complex Reveals an Asymmetric Target Binding Mechanism. *Proc. Natl. Acad. Sci. U.S.A.* **2012**, *109*, 6048−6053.
(53) Berendsen, H. J. C.; van der Spoel, D.; van Drunen, R. GROMACS: A Message-Passing Parallel Molecular Dynamics Implementation. *Comput. Phys. Commun.* **1995**, *91*, 43−56.
(54) Lindahl, E.; Hess, B.; van der Spoel, D. GROMACS 3.0: A Package for Molecular Simulation and Trajectory Analysis. *J. Mol. Model.* **2001**, *7*, 306−317.
(55) Van Der Spoel, D.; Lindahl, E.; Hess, B.; Groenhof, G.; Mark, A. E.; Berendsen, H. J. C. GROMACS: Fast, Flexible, and Free. *J. Comput. Chem.* **2005**, *26*, 1701−1718.
(56) Hess, B.; Kutzner, C.; Van Der Spoel, D.; Lindahl, E. GRGMACS 4: Algorithms for Highly Efficient, Load-Balanced, and Scalable Molecular Simulation. *J. Chem. Theory Comput.* **2008**, *4*, 435−447.
(57) Pronk, S.; Páll, S.; Schulz, R.; Larsson, P.; Bjelkmar, P.; Apostolov, R.; Shirts, M. R.; Smith, J. C.; Kasson, P. M.; Van Der Spoel, D.; et al. GROMACS 4.5: A High-Throughput and Highly Parallel Open Source Molecular Simulation Toolkit. *Bioinformatics* **2013**, *29*, 845−854.
(58) Lindorff-Larsen, K.; Piana, S.; Palmo, K.; Maragakis, P.; Klepeis, J. L.; Dror, R. O.; Shaw, D. E. Improved Side-Chain Torsion Potentials for the Amber Ff99SB Protein Force Field. *Proteins: Struct., Funct., Bioinf.* **2010**, *78*, 1950−1958.
(59) Jorgensen, W. L.; Chandrasekhar, J.; Madura, J. D.; Impey, R. W.; Klein, M. L. Comparison of Simple Potential Functions for Simulating Liquid Water. *J. Chem. Phys.* **1983**, *79*, 926−935.
(60) Hess, B.; Bekker, H.; Berendsen, H. J. C.; Fraaije, J. G. E. M. LINCS: A Linear Constraint Solver for Molecular Simulations. *J. Comput. Chem.* **1997**, *18*, 1463−1472.
(61) Miyamoto, S.; Kollman, P. A. Settle: An Analytical Version of the SHAKE and RATTLE Algorithm for Rigid Water Models. *J. Comput. Chem.* **1992**, *13*, 952−962.
(62) van Gunsteren, W. F.; Berendsend, H. J. A Leap Frog Algorithm for Stochastic Dynamics. *Mol. Simul.* **1988**, *1*, 173−185.
(63) Bussi, G.; Donadio, D.; Parrinello, M. Canonical Sampling through Velocity Rescaling. *J. Chem. Phys.* **2007**, *126*, No. 014101.
(64) Berendsen, H. J. C.; Postma, J. P. M.; Van Gunsteren, W. F.; Dinola, A.; Haak, J. R. Molecular Dynamics with Coupling to an External Bath. *J. Chem. Phys.* **1984**, *81*, 3684−3690.
(65) Parrinello, M.; Rahman, A. Polymorphic Transitions in Single Crystals: A New Molecular Dynamics Method. *J. Appl. Phys.* **1981**, *52*, 7182−7190.
(66) Essmann, U.; Perera, L.; Berkowitz, M. L.; Darden, T.; Lee, H.; Pedersen, L. G. A Smooth Particle Mesh Ewald Method. *J. Chem. Phys.* **1995**, *103*, 8577−8593.
(67) Carlsson, J.; Åqvist, J. Absolute and Relative Entropies from Computer Simulation with Applications to Ligand Binding. *J. Phys. Chem. B* **2005**, *109*, 6448−6456.
(68) Karplus, M.; Kushick, J. N. Method for Estimating the Configurational Entropy of Macromolecules. *Macromolecules* **1981**, *14*, 325−332.
(69) Yildirim, A.; Tekpinar, M.; Wassenaar, T. A. Molecular Dynamics Investigation of Helicobacter Pylori Chemotactic Protein CheY1 and Two Mutants. *J. Mol. Model.* **2014**, *20*, No. 2212.
(70) Tekpinar, M.; Yildirim, A.; Wassenaar, T. A. Molecular Dynamics Study of the Effect of Active Site Protonation on

https://doi.org/10.1021/acs.jpcb.1c02096
J. Phys. Chem. B 2021, 125, 10059−10071

Helicobacter Pylori 5′-Methylthioadenosine/S-Adenosylhomocysteine Nucleosidase. *Eur. Biophys. J.* **2015**, *44*, 685−696.
(71) Lange, O. F.; Grubmüller, H. Generalized Correlation for Biomolecular Dynamics. *Proteins: Struct., Funct., Bioinf.* **2005**, *62*, 1053−1061.

https://doi.org/10.1021/acs.jpcb.1c02096
J. Phys. Chem. B 2021, 125, 10059−10071